JOURNAL OF MATERIALS SCIENCE 22 (1987) 2599–2608

High-temperature strength and ductility of $L1_2$-type Ni_3Al–Ni_3Mn intermetallic compound

N. MASAHASHI, T. TAKASUGI, O. IZUMI
The Research Institute for Iron, Steel and Other Metals, Tohoku University, Sendai, Japan

The mechanical properties of $L1_2$-type pseudobinary intermetallic compound Ni_3Al–Ni_3Mn were investigated in relation to testing temperature and alloy composition. A positive temperature dependence of yield stress was found in manganese compositions lower than 15 at%, suggestive of the Kear–Wilsdorf mechanism, while a negative dependence was found in the high manganese alloys. The composition dependence of yield stress at room temperature in the low manganese alloys was attributed to the solid solution hardening while that in the high manganese alloys was attributed to imperfect ordering. The elongation exhibited a maximum around 700 K irrespective of compositions, while the maximum and minimum were observed approximately in 9 and 12 at% manganese alloys, respectively. The high values of elongation obtained in 20 and 25 at% manganese alloys were probably due to imperfect ordering. Both the temperature and composition dependences of UTS were quite similar to those of elongation. The fractographic observation showed that the more ductile specimen tended to fracture more transgranularly.

1. Introduction

The mechanical properties of $L1_2$-type intermetallic compound have been regarded with great interest because some of these compounds show an anomalous increase of yield stress at elevated temperature [1–4]. Ni_3Al is the most extensively studied of the $L1_2$-type intermetallic compounds. Its yield stress attains six- to seven-fold at peak temperature (around 1000 K) compared with that at room temperature. This characteristic has been used practically as a precipitated strengthening phase in a nickel-base superalloy. In addition to this anomalous strengthening, excellent oxidation and creep resistances have made it an attractive structural material for operation at high temperatures [5, 6]. However, the intrinsically brittle tendency of grain boundaries has prevented it from practical uses. The grain boundaries of Ni_3Al are inherently fragile due to poor grain-boundary cohesion. Studies of fracture surfaces in high-purity Ni_3Al indicated intergranular failure without appreciable segregation of impurities at grain boundaries [7, 8]. Based on the atomistic consideration in the grain-boundary region of the $L1_2$-type compound, it was suggested that the heterogeneous bonding environment at the grain-boundary region is responsible for the poor cohesive strength and thereby the brittle intergranular fracture [9, 10].

Recently, vigorous efforts have been made to improve the ductility of Ni_3Al, adopting new material processings such as the hydrostatic pressure technique coupled with powder metallurgy [11] and the rapid solidification technique [12], and also using alloy design based on physical metallurgy principles. In the latter approach, Aoki and Izumi first discovered a significant ductility improvement of Ni_3Al at room temperature by addition of small amounts of boron [13, 14]. It was subsequently shown by Auger experiment [15] that the boron segregated strongly to grain boundaries and then resulted in an increase in the cohesive strength of the grain boundary, and is therefore effective by "micro" alloying. In addition, Takasugi *et al.* [10] found that a transition metal of manganese or iron which can substitute for aluminium sites is effective in improving the ductility of Ni_3Al. It was suggested, based on the atomistic consideration at the Ni_3Al grain boundary that these third elements create a homogeneous environment regarding electronic chemical bonding at grain-boundary cohesion. Therefore, this effect should be effective by "macro" alloying.

The mechanical properties of Ni_3Al ductilized on the above principles must be investigated systematically as a function not only of alloy composition but also of testing temperature. In addition, it is essential to know the strength properties, ductility behaviour and fracture behaviour in tension for the evaluation of the optimum conditions for application. In this paper, the mechanical properties of Ni_3Al macro-alloyed with manganese are described. The manganese element is a transition metal of group VIIa in the Periodic Table and constitutes $L1_2$-type ordered structure with the nickel atom (Ni_3Mn). Ni_3Mn also has an order–disorder transformation point (T_c) at 770 K [16, 17]. According to our investigation of the partial phase diagram for the Ni–Al–Mn alloy system, this alloy system forms a continuous solid solution at low-temperature regions and is therefore represented as $Ni_3(Al, Mn)$ on the Ni_3Al–Ni_3Mn pseudobinary line [18]. From the formation of the continuous solid solution of $Ni_3(Al, Mn)$, it is expected that the

0022–2461/87 $03.00 + .12

mechanical properties change from Ni_3Al to Ni_3Mn continuously rather than discontinuously; the strength of the extreme composition of Ni_3Al is well characterized by a positive temperature dependence. This behaviour was attributed to the dislocation immobilization by the cross-slip of $\langle 1\,1\,0 \rangle$ screw dislocations from the primary $\{1\,1\,1\}$ plane to the $\{1\,0\,0\}$ plane, the so-called Kear–Welsdorf mechanism [19]. The cross-slip is driven by the APB energy anisotropy between those two planes. With increasing manganese substituting for aluminium, it is expected that the ductility will increase and, contrarily, the anomalous behaviour of strength will tend to diminish. Because the ordering energy of Ni_3Mn is low compared with that of Ni_3Al, an increase of manganese concentration will reduce the APB energy on $\{1\,1\,1\}$, and produce less frequent cross-slip, thus resulting in a diminishing of the positive temperature dependence of strength. The strength of another extreme composition of Ni_3Mn shows a negative temperature dependence and draws a sharp peak just below T_c [20, 21]. Ni_3Mn is ductile and fractures by the transgranular fracture mode [9].

In the present work, the mechanical properties (strength, elongation and fracture) of $L1_2$-type Ni_3Al–Ni_3Mn pseudobinary alloys were examined by the tension test. The major objective was to determine the effects of alloy composition and testing temperature on these mechanical properties.

2. Experimental procedure

The purity of materials used in this experiment was 99.95 wt % nickel, 99.9 wt % manganese and 99.99 wt % aluminium. The ingot buttons were prepared by arc-melting using a non-consumable tungsten electrode in argon gas atmosphere. The buttons were remelted several times by turning over in order to attain chemical homogeneity. The weight losses during melting were less than 0.2 wt %. Chemical analysis showed little differences between nominal and analysed values. Therefore, the alloys used in this work are expressed as the nominal compositions. The selected compositions were 6, 9, 12, 15, 20, and 25 at % manganese. All buttons were homogenized for 172.8 ksec at 1323 K under vacuum ($< 1.3 \times 10^{-3}$ Pa), followed by furnace cooling. All buttons were then cut into rectangular bars using a slitting wheel cutter and then heat-treated to achieve sufficient ordering under vacuum; 1323 K, 86.4 ksec → 1073 K, 172.8 ksec → 773 K, 259.2 ksec (723 K, 432 ksec for Ni_3Mn), followed by furnace cooling. The tensile specimens of 2.5 mm diameter and 22.5 mm gauge length were prepared from these bars using a turning lathe. The tensile specimens were evacuated in quartz tubes under vacuum and then annealed at 1323 K for 86.4 ksec and then at 773 K for 259.2 ksec (at 723 K for 259.2 ksec for Ni_3Mn) to remove residual strains due to machining and also to establish full ordering, followed by furnace cooling. The tensile tests were made using an Instron-type testing machine at a nominal strain rate of $1.1 \times 10^{-4}\,sec^{-1}$. The room-temperature tests were performed in air while the elevated temperature tests up to 1073 K were conducted in a vacuum of 1.3×10^{-3} Pa. After testing, the fracture surfaces of the specimens were examined by scanning electron microscopy (SEM). Metallographic observation and X-ray analysis were also conducted.

3. Experimental results

3.1. Microstructure and crystallography

The microstructure depended on the composition; with an increase of manganese concentration, the morphology changed from columnar to equi-axed grains. The twin boundaries were frequently found in alloys with high manganese concentration. Figs 1a, b and c show the microstructures of 6, 12 and 25 at % Mn (Ni_3Mn), respectively. X-ray analysis confirmed the presence of the $L1_2$ single phase without

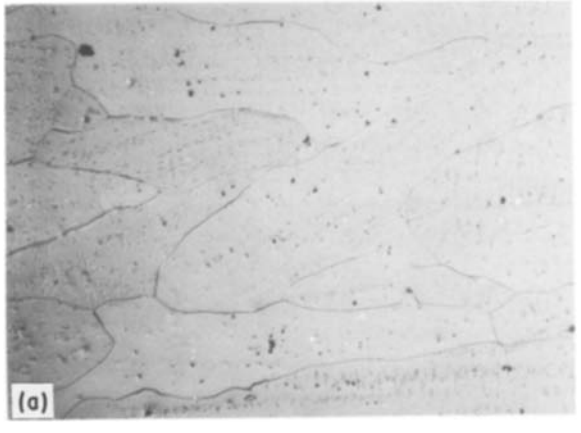

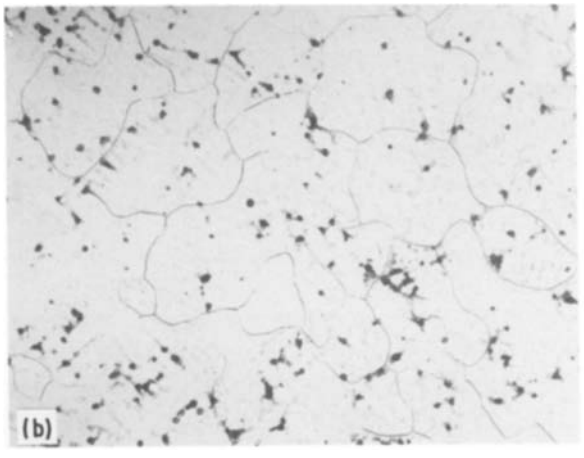

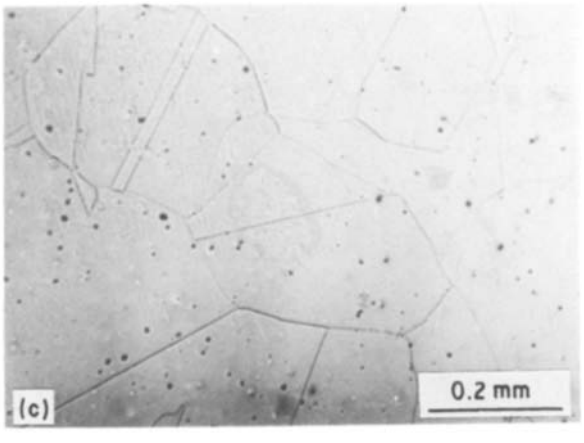

Figure 1 Optical microstructures of (a) 6 at % Mn, (b) 12 at % Mn and (c) 25 at % Mn alloys.

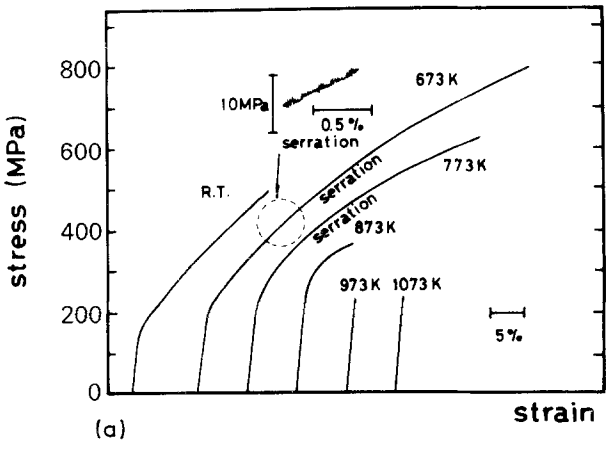

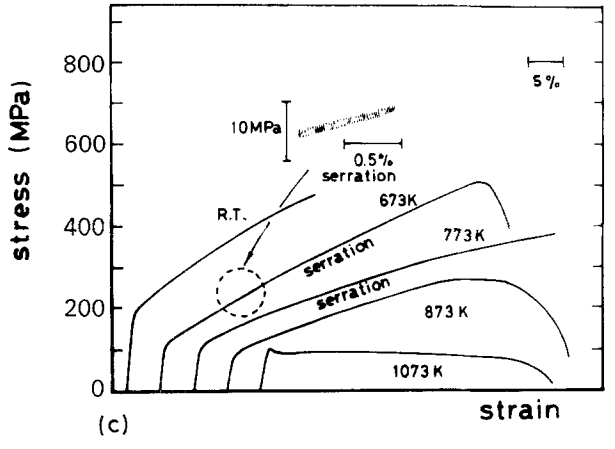

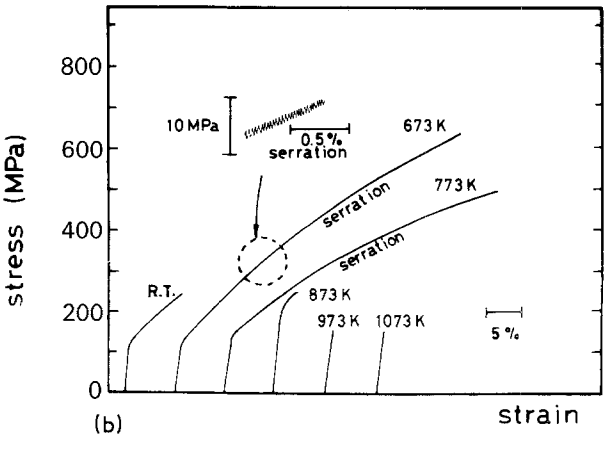

Figure 2 Nominal stress–strain curves at various temperatures for (a) 9 at % Mn, (b) 15 at % Mn and (c) 25 at % Mn alloys.

any second phases. The lattice parameter changed continuously with composition (see [18]).

3.2. Mechanical properties

Figs 2a, b and c representatively show the nominal stress–strain curves at various temperatures for 9, 15 and 25 at % Mn alloys, respectively. Note that all of the tested alloys exhibited tensile elongations (ductilities) over a wide range of testing temperatures. As the manganese concentration increases, the work-hardening rate decreased moderately. It is also noted that the stress–strain curves of specimens tested at intermediate temperatures (i.e. 673 and 773 K) showed serrations. The serrations appeared more frequently and intensively in alloys containing higher manganese concentrations.

Figs 3 and 4 illustrate the variations of the 0.2% flow stress (i.e. yield stress) as a function of testing temperature and of manganese concentration, respectively. As some of the tensile specimens fractured within the elastic region especially at high temperatures and/or in low manganese composition alloys, the corresponding data were not obtained (see Fig. 2). From the yield stress against temperature curves (Fig. 3), the positive temperature dependence of yield stress was clearly found in alloys containing a manganese concentration lower than 15 at % Mn. This temperature dependence, as expected, tended to be less remarkable with increasing manganese concentration. Although the peak temperatures in the stress against temperature curves were not determined in these alloys, they are suggested to be at or above 873 K. With further increases of manganese concentration (i.e. in 20 and 25 at % Mn), negative temperature dependences of yield stress were found instead. In 20 at % Mn alloy, a small increase of yield stress was preceded by a negative temperature dependence. Also, in extreme compositions of the 25 at % Mn alloy, a faint plateau was shown at 773 K. This behaviour will be discussed later. The yield stress–composition behaviour (Fig. 4) at room temperature showed that yield stress increased to a maximum at 12 at % Mn, decreased to a minimum at 15 at % Mn, then again increased to a high value at the extreme composition

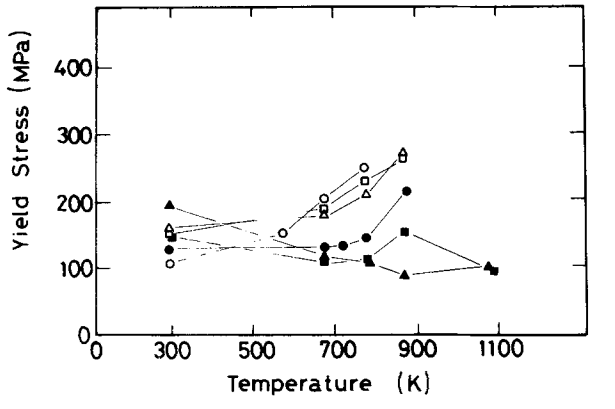

Figure 3 Temperature dependence of yield stress for (○) 6, (□) 9, (△) 12, (●) 15, (■) 20, and (▲) 25 at % Mn alloys.

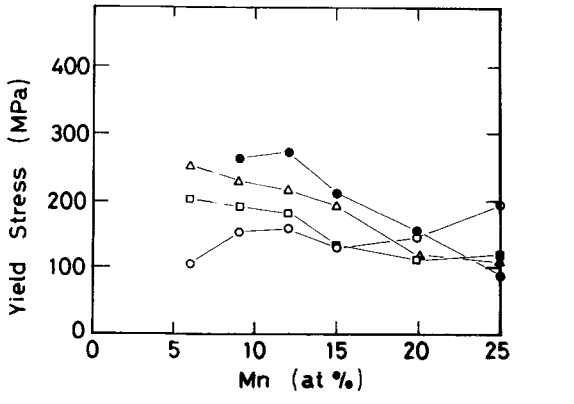

Figure 4 Composition dependence of yield stress at (○) RT, (□) 673 K, (△) 773 K, and (●) 873 K.

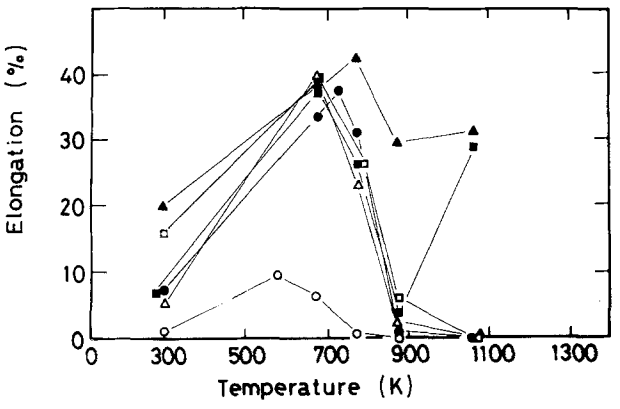

Figure 5 Temperature dependence of elongation for (○) 6, (□) 9, (△) 12, (●) 15, (■) 20, (▲) 25 at % Mn alloys.

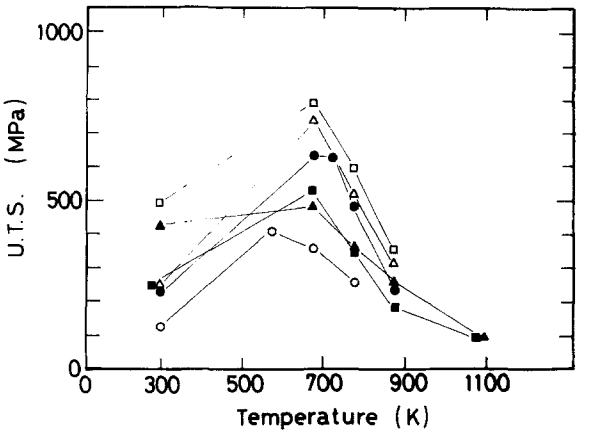

Figure 7 Temperature dependence of ultimate tensile stress (UTS) for (○) 6, (□) 9, (△) 12, (●) 15, (■) 20, (▲) 25 at % Mn alloys.

of 25 at % Mn. The maximum at 12 at % Mn is postulated to be due to the solid solution hardening by mixing aluminium and manganese atoms, while the high value at Ni_3Mn might be attributable to the imperfect ordering of this alloy. Thus, it is suggested that the yield stresses of the Ni_3Al–Ni_3Mn alloys at ambient temperatures are primarily controlled by the athermal component. As the testing temperature increases, the yield stresses showed higher values at low manganese concentrations, suggesting the operation of the thermally activated process of Kear–Wilsdorf (cross-slip) mechanism [19].

Figs 5 and 6 show the variation of elongation as a function of testing temperature and manganese concentration, respectively. Elongation increased from room temperature to a maximum, and then decreased in the alloys containing manganese concentrations lower than 15 at % Mn (Fig. 5). The temperature at which maximum elongation appeared tended to be higher as the manganese concentration increased (573 K at 6 at % Mn to 773 K at 15 at % Mn). However, in two alloys containing higher manganese concentrations (i.e. 20 and 25 at % Mn) the elongations again increased at sufficiently high temperatures, i.e. at 1073 K. From Fig. 6 it is seen that the elongation increases from 6 at % Mn to a maximum around 9 at % Mn, decreases to a shallow minimum at 12 or 15 at % Mn and again increases up to the extreme composition of 25 at % Mn. This behaviour is basically insensitive to testing temperature.

Figs 7 and 8 show the ultimate tensile stress (UTS) as a function of the testing temperature and manganese concentration, respectively. Fig. 7 shows that the UTS increased from room temperature to a maximum and then decreased, with increasing temperature. The peak temperature was found at 673 K except for 6 at % Mn alloy (i.e. 573 K). In Fig. 8, the UTS shows a maximum at 9 at % Mn alloy irrespective of testing temperature. Also, in the alloy with the extreme composition of 25 at % Mn, the UTS at room temperature and 873 K again increased. Here, it should be noted that the fact that the temperature dependence and compositional dependence of UTS were quite similar to those of the elongation suggests a close relationship between the two properties.

3.3. Fracture behaviour

SEM observation exhibited a variety of fracture modes, depending on the testing temperature and composition. The fractographs tested at room temperature, 673 and 873 K, for a series of compositions are shown in Figs 9a to h, 10a to h and 11a to h, respectively. The fractographs tested at room temperature are strongly influenced by alloy composition. For low manganese alloys (i.e. 6 and 9 at % Mn), the fracture surface is heterogeneous and embossed with the original grain morphology, i.e. columnar grains. The fracture surface of the 6 at % Mn alloy (Figs 9a

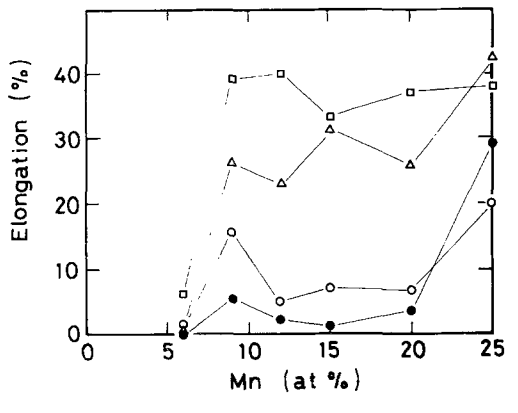

Figure 6 Composition dependence of elongation at (○) RT, (□) 673 K, (△) 773 K, (●) 873 K.

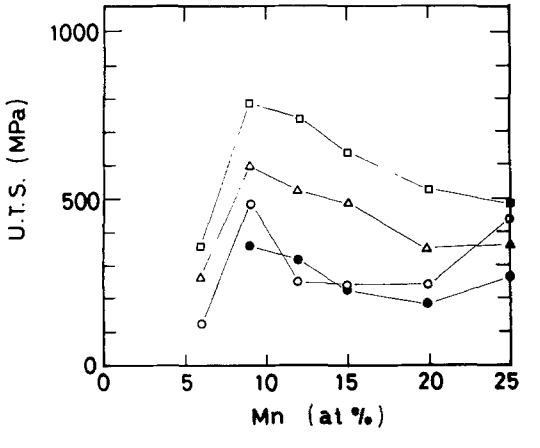

Figure 8 Composition dependence of ultimate tensile stress (UTS) at (○) RT, (□) 673 K, (△) 773 K, (●) 873 K.

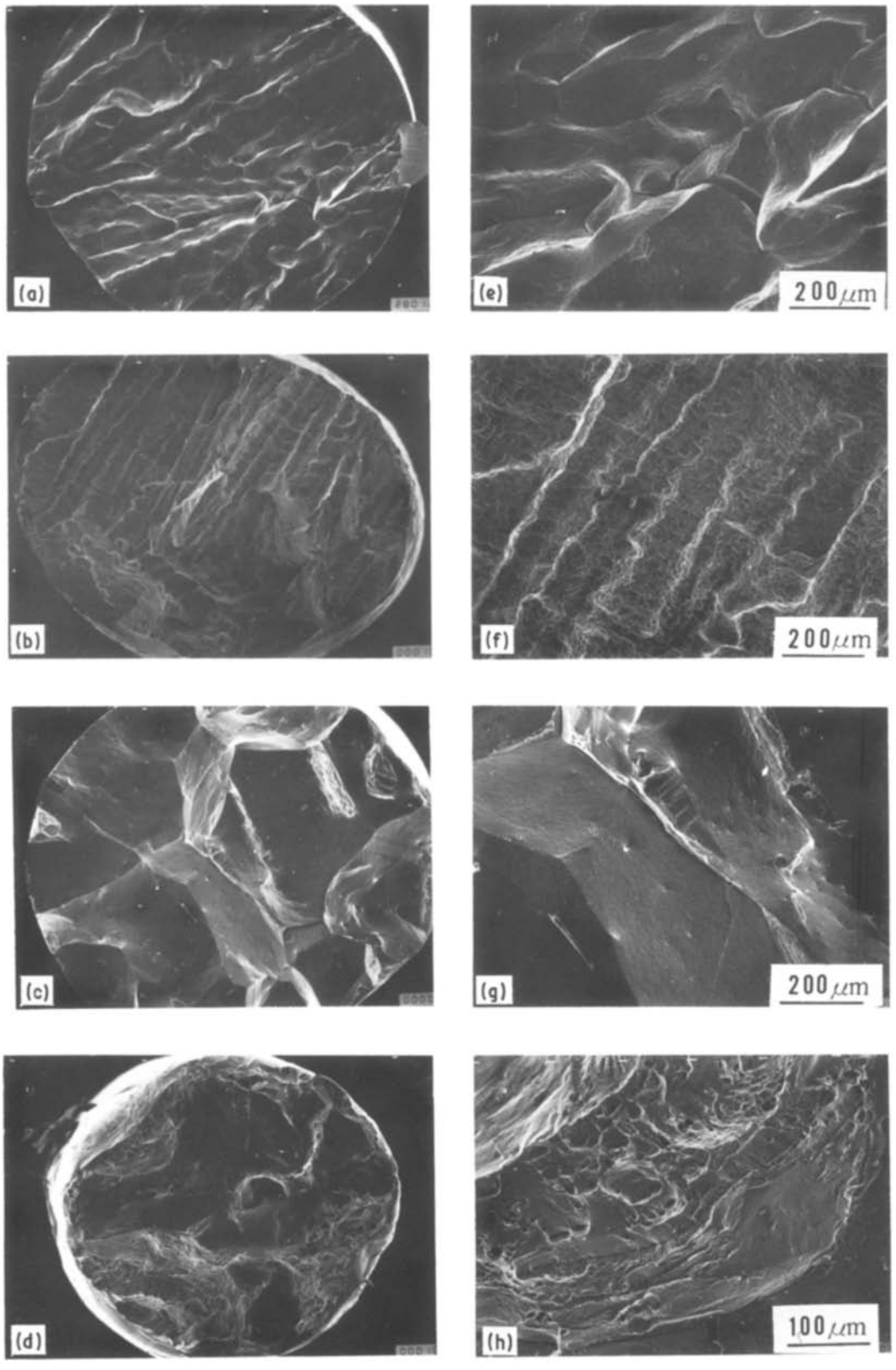

Figure 9 SEM fractographs tested at room temperature for (a) and (e) 6 at % Mn, (b) and (f) 9 at % Mn, (c) and (g) 12 at % Mn and (d) and (h) 25 at % Mn alloys.

and e) showed smooth grain-boundary facets mixed with a small amount of the transgranular fracture mode. The alloy of 9 at % Mn (Figs 9b and f) showed an almost transgranular fracture surface. In intermediate manganese alloys (i.e. 12 at % Mn), the smooth grain-boundary facets were mixed with a minority of the transgranular fracture surfaces (Figs 9c and g). The 25 at % Mn alloy (Ni_3Mn) exhibited a completely transgranular fracture mode showing a dimple pattern (Figs 9d and h). Thus, the correlation between the ductility (Fig. 6) and the fracture mode (Fig. 9) is clear at room temperature; that is, the alloys showing the transgranular fracture patterns (i.e. 9 at % Mn and 15 at % Mn) exhibited the higher values of elongation.

In the fractographs tested at intermediate temperatures (i.e. 673 K) where the ductility recorded was almost a maximum, the transgranular fracture modes

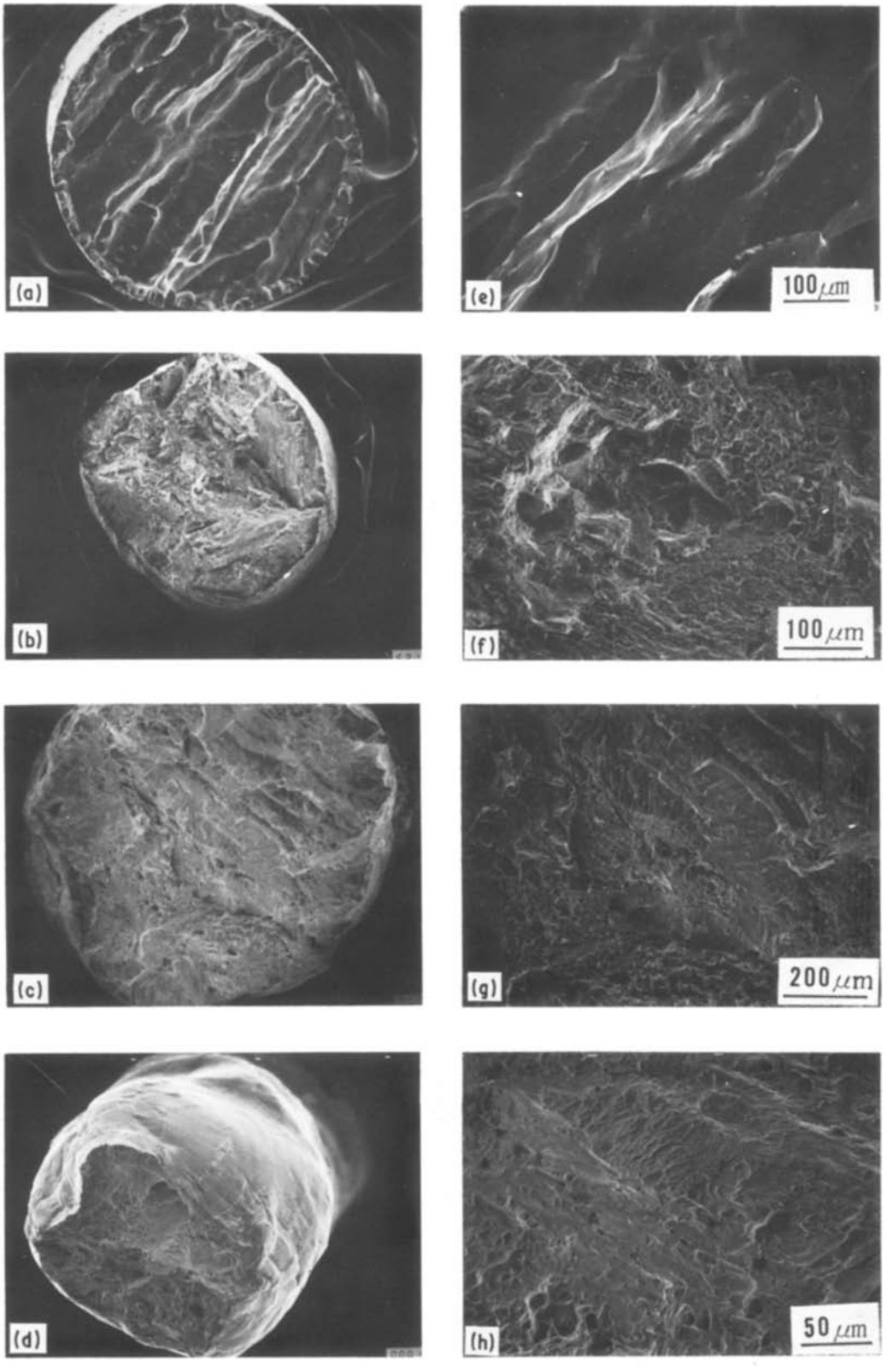

Figure 10 SEM fractographs tested at 673 K for (a) and (e) 6 at % Mn, (b) and (f) 9 at % Mn, (c) and (g) 12 at % Mn and (d) and (h) 25 at % Mn alloys.

showing the dimple patterns were dominant for every alloy, except for the 6 at % Mn alloy. In the 6 at % Mn alloy (Figs 10a and e), the fracture surfaces exhibited smooth grain-boundary facets on which some small voids (cavities) were occasionally observed. In the other remaining alloys, completely transgranular fracture modes were seen (Figs 10b to d and f to h). In the alloys showing high ductilities, the reductions in cross-sectional areas of specimen were very large, i.e. marked neckings were found.

The fracture mode in specimens tested at 873 K changed in a similar way to those seen at room temperature, which showed a strong dependence on the alloy composition. In the 6 at % Mn alloy (Figs 11a and e), the grain-boundary facets were smooth and showed little trace of deformation. In the 9 at % Mn alloy (Figs 11b and f), fractography showed a mixed mode of intergranular and the transgranular fracture. In the 12 at % Mn alloy (Figs 11c and g), the intergranular fracture mode again governed the fracture

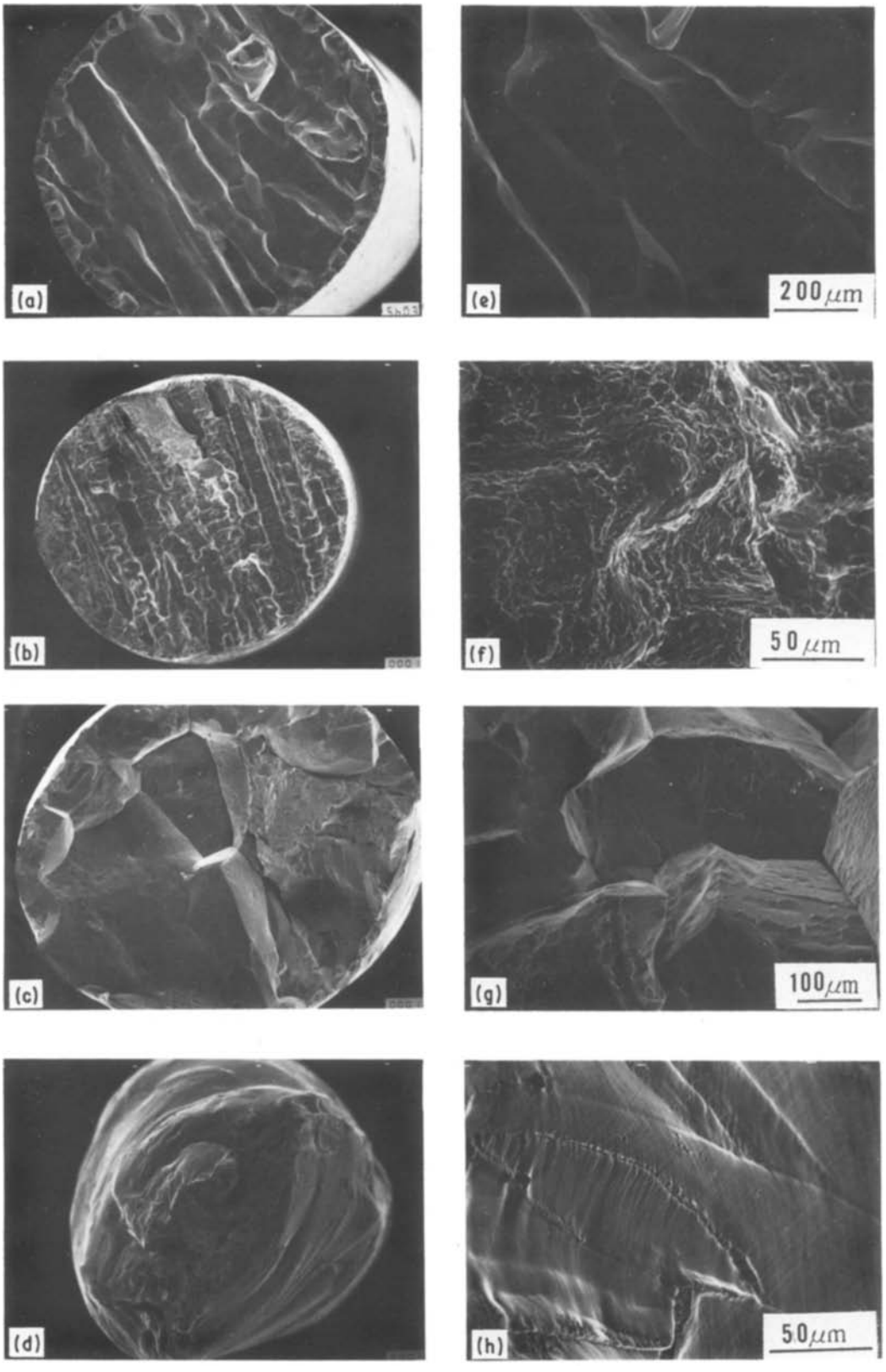

Figure 11 SEM fractographs tested at 873 K for (a) and (e) 6 at % Mn, (b) and (f) 9 at % Mn, (c) and (g) 12 at % Mn and (d) and (h) 25 at % Mn alloys.

surface. With further increase of manganese (i.e. 20 and 25 at % Mn), the fracture surfaces were dominated by the transgranular fracture mode (Figs 11d and h). Thus, the correlation between ductility and fracture mode is again recognized at 873 K (compare Fig. 6 with Fig. 11).

At 1073 K, most specimens containing less than 15 at % Mn fractured intergranularly while the high manganese content alloys (i.e. 20 and 25 at % Mn) showed a large number of small dimple patterns (Figs 12a and b), reflecting the high ductilities shown in Fig. 5.

4. Discussion

The mechanical properties of the Ni_3Al–Ni_3Mn alloys observed in this work, as expected in Section 1, changed continuously rather than discontinuously in terms not only of the compositional dependence but also of the

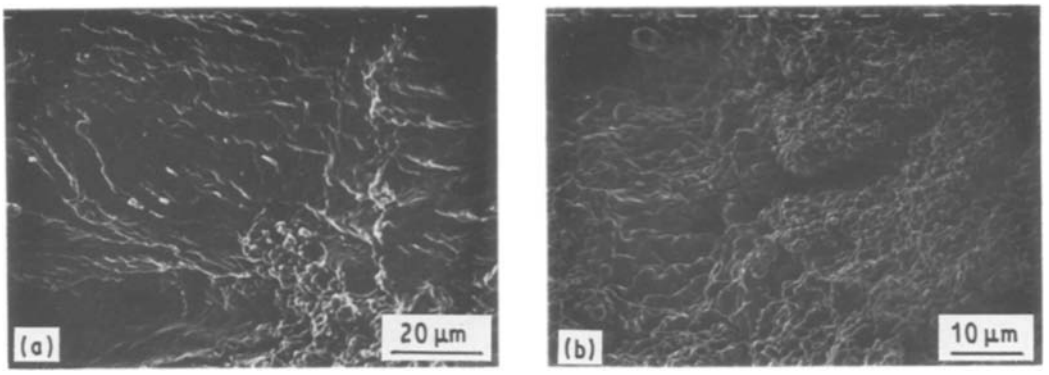

Figure 12 SEM fractographs tested at 1073 K for (a) 20 at % Mn and (b) 25 at % Mn alloys.

testing temperature dependence. However, it should be noted that this behaviour is not so monotonic but is complex. The result suggests that the dependences of these mechanical properties on composition are basically divided into two areas; one is the area (from 0 to 15 at % Mn) affected by the nature of the extreme alloy of Ni_3Al and another is the area (from 20 to 25 at % Mn) affected by the nature of the extreme alloy of Ni_3Mn. Thus, it is suggested that the critical composition separating the two areas corresponds approximately to 15 to 20 at % Mn.

First, we discuss the yield stress properties. As shown in Fig. 4, a maximum yield stress at room temperature was found at 12 at % Mn. This result indicates that the solid solution hardening by mixing aluminium and manganese atoms is symmetrical, because a peak appeared almost at equi-atomic compositions of both atoms, i.e. $Ni_3(Al_{0.5}, Mn_{0.5})$. The high value of the room-temperature yield stress in the 25 at % Mn alloy (Ni_3Mn) may be attributable to the imperfect ordering, because in order to attain the fully ordered structure in this alloy, a prolonged heat treatment should be taken below T_c (770 K). It is generally recognised that partially ordered structure produces the resistant stress against moving dislocations, resulting in a higher strength. Fig. 13 schematically shows two contributions involved in the yield stress (σ_y) of the Ni_3Al–Ni_3Mn alloys; one is the solid solution hardening (σ_1) and another is the hardening due to the imperfect ordering (σ_2).

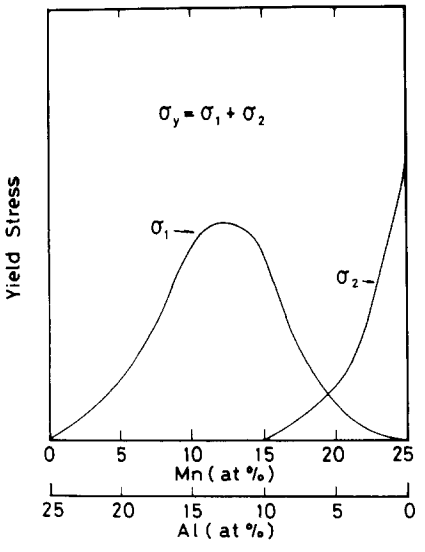

Figure 13 Schematic illustration of two contributions involved in the room-temperature yield stress (σ_y) of the Ni_3Al–Ni_3Mn alloys. Note that σ_1 is due to the solid solution hardening and σ_2 is due to disordering hardening.

When the yield stress is plotted against testing temperature (Fig. 3), a positive temperature dependence was shown at low manganese concentrations, suggesting operation of the Kear–Wilsdorf mechanism [19]. The monotonic decrease in the slope of the positive temperature dependence with increasing manganese concentration is attributed to the lowering of the APB energy anisotropy by the addition of the manganese atom. This trend is thus consistent with the lowering of the transformation temperature from the $L1_2$ structure (γ') to fcc disordered structure (γ) in the partial phase diagram of the Ni_3Al–Ni_3Mn pseudobinary system [18]. In general, this temperature is proportional to the ordering energy, i.e. the APB energy of alloys. On the other hand, the slight increase of yield stress at 873 K in the 20 at % Mn alloy is not attributed to the Kear–Wilsdorf process but to the effect of the partial disordering below T_c. The partial phase diagram along Ni_3Al–Ni_3Mn indicated that T_c at 20 at % Mn is approximately 900 K [18].

Next, we discuss the ductility properties. As shown in Fig. 6, the ductility becomes observable at about 6 at % Mn at every testing temperature. This result suggests that the strengthening of the grain boundaries becomes effective by the substitution of one fifth of the manganese atoms for aluminium atoms. In other words, the electronic chemical bonding environment in the grain-boundary region becomes homogeneous from this composition, thus suppressing the easier intergranular fracture. The shallow elongation minimum at about 12 to 15 at % Mn corresponds to the equi-atomic composition of aluminium and manganese atoms, i.e. $Ni_3(Ai_{0.5}, Mn_{0.5})$ along the Ni_3Al–Ni_3Mn pseudobinary line. If we assume that the grain boundary in the alloy having a higher-ordered crystal structure, like $Ni_3Al_{0.5}Mn_{0.5}$, is more fragile than that of a lower-ordered crystal structure, like $Ni_3(Al, Mn)$, the grain-boundary cohesive strength could be poor at this composition and may result in lower ductility. However, to validate this assumption for the correlation between grain-boundary strength and crystal structure, extensive studies will be required. The high value of elongation at 25 at % Mn (Ni_3Mn) not only at ambient temperature but also at elevated temperature, is again attributed to the imperfect ordering

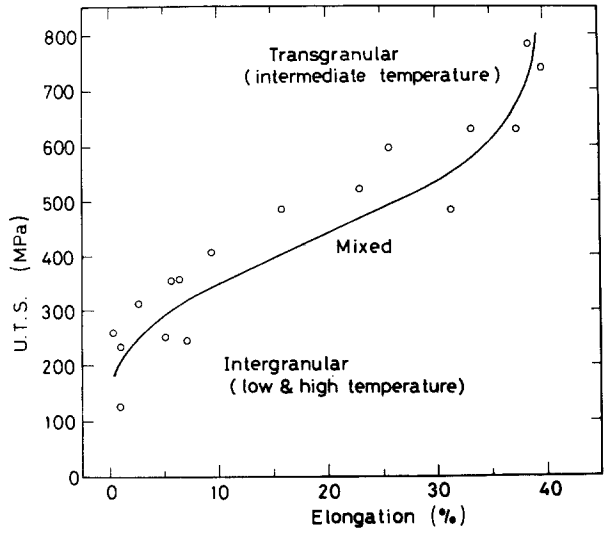

Figure 14 Relationship between elongation and ultimate tensile stress (UTS).

below T_c and disordered crystal structure (fcc) above T_c. It is generally accepted that the grain boundary in the disordered state is stronger than that in the ordered state.

As shown in Fig. 5, the ductility showed a maximum at around 700 K for every alloy. Here, we must remember that the tensile test at room temperature was conducted in air, whereas that at the remaining temperatures was conducted in vacuum. Studies on some $L1_2$-type ordered alloys have shown that hydrogen greatly affects their ductility and generally causes embrittlement by reducing the grain-boundary cohesive strength [22]; this embrittlement can be seen in the samples which were deformed in air atmosphere, at ambient temperatures and at slow strain rates. Therefore, the primary reason for the low ductility of the present alloys at room temperature is attributed to hydrogen embrittlement. An extensive study of this subject has been done on the present alloys and will be described in a subsequent paper [23]. On the other hand, the lowering of elongation beyond the peak temperature might be due to the cavitation damage which appeared on the grain-boundary facets. Because this damage is created by vacancy flow and/or creep flow, it has to be effective at elevated temperatures.

We investigated the tight correlation between the properties of elongation, UTS and fracture mode. Fig. 14 clearly indicates that there is a good correlation between elongation and UTS; higher elongations produced higher UTS. Therefore, it is suggested that both mechanical properties are induced from the same origin (mechanism), i.e. effected through the fracture mode. In the region in which the intergranular fracture mode is dominant, the UTS increased steeply with increasing elongation; in the region in which fracture is a mixture of inter- and the transgranular fractures, the UTS increased slowly with increasing elongation; finally, in the region in which the transgranular fracture mode is dominant, the UTS again increased rapidly with increasing elongation. The first region was observed in samples tested at both low and high temperatures while the last region was observed in samples tested at intermediate temperatures. Thus, the grain boundary strengthened by the testing temperature effect or by the alloying effect suppresses the intergranular fracture and thereby guarantees the deformation of the grain interior, resulting in higher elongation and simultaneously higher UTS of the alloy.

Serrations appeared at the intermediate temperatures where maximum elongations were usually attained. Generally, the occurrence of serrations was considered to be due to the interaction between moving dislocations and solute atoms (i.e. Portevin-Le Chatelier effect) [24]. In the case of low manganese alloys, the manganese atoms substituting for aluminium are expected to interact with dislocations. Hence, the diffusivity of manganese atoms, i.e. D_{Mn}, is an important controlling factor in the present phenomenon. However, no data for this value are available. In the 20 and 25 at % Mn alloys, strong serrations appeared at 673 K just below T_c. In this case, the diffusivity of aluminium, i.e. D_{Al}, might control the plastic flow at intermediate temperatures. However, the occurrence of strong serrations of the Ni_3Mn alloy just below T_c is postulated to be affected by imperfect ordering coupled with solute atoms.

5. Conclusions

The $L1_2$-type Ni_3Al–Ni_3Mn pseudobinary intermetallic compounds were tensile tested from room temperature to 1073 K, in relation to their composition. The yield stress, tensile elongation and ultimate tensile stress (UTS) were correlated with the fracture behaviour. The results obtained in this work are given below.

1. The yield stress at room temperature is controlled by the athermal component of solid solution hardening in the low manganese concentration range, and of the hardening due to the imperfect ordering in the high manganese concentration range.

2. The positive temperature dependence of yield stress was observed in alloys containing less than 15 at % manganese suggestive of the operation of the thermal process of the Kear–Wilsdorf mechanism. Within this composition range the positive temperature dependence was larger in the sequence 6 at % Mn > 9 at % Mn > 12 at % Mn > 15 at % Mn alloys. A slight increase in yield stress just below T_c in the high manganese alloys was attributable to the interaction of dislocations with imperfect ordering.

3. Over a wide range of testing temperatures, the tensile elongation showed a maximum and minimum at compositions of 9 and 12 at % Mn, respectively, when plotted as a function of composition. Tensile elongation, when plotted as a function of testing temperature, also showed a maximum at intermediate temperatures (673 to 773 K) over a wide range of manganese concentrations. The former variation was attributed to the change of the grain-boundary cohesive strength with composition. The latter variation was induced by the introduction of intergranular hydrogen embrittlement at low temperatures and of intergranular creep damage at elevated temperatures. The higher values of elongation observed in the extreme composition of Ni_3Mn and were attributed to

imperfect ordering below T_c and to the disordered structure above T_c.

4. The UTS changed in a quite similar way to elongation in terms not only of testing temperature but also of chemical composition, suggestive of the operation of the same mechanisms as those appearing in elongation behaviour.

5. Fractographic observation indicated that a strong correlation existed between fracture mode, elongation and UTS. With an increase in elongation and UTS, the fracture mode changed from intergranular- to transgranular fracture.

Acknowledgements

We wish to thank Messrs K. Sasamori and K. Saito for specimen preparation and S. Ogi for X-ray diffraction measurement.

References

1. P. A. FLINN, *Trans. Met. Soc. AIME* **218** (1960) 145.
2. R. G. DAVIES and N. S. STOLOFF, *Trans. Met. Soc. AIME* **233** (1965) 714.
3. S. M. COPLEY and B. H. KEAR, *ibid.* **239** (1967) 977.
4. P. H. THORNTON, R. G. DAVIES and T. L. JOHNSON, *Metall. Trans.* **1** (1970) 207.
5. J. H. WESTBROOK, "Mechanical Properties of Intermetallic Compounds", edited by J. H. Westbrook (Wiley, 1960) p. 1.
6. A. LAWLY, "Intermetallic Compound", edited by J. H. Westbrook (Wiley, 1967) p. 464.
7. T. TAKASUGI, E. P. GEORGE, D. P. POPE and O. IZUMI, *Scripta Metall.* **19** (1984) 551.
8. T. OGURA, S. HANADA, T. MASUMOTO and O. IZUMI, *Met. Trans. A* **16A** (1985) 441.
9. T. TAKASUGI and O. IZUMI, *Acta Metall.* **33** (1985) 1247.
10. T. TAKASUGI, O. IZUMI and N. MASAHASHI, *ibid.* **33** (1985) 1259.
11. I. BAKER, D. V. VIENS and E. M. SCHULSON, *Scripta Metall.* **18** (1984) 237.
12. A. INOUE, H. TOMIOKA and T. MASUMOTO, *Met. Trans. A* **14A** (1983) 1367.
13. K. AOKI and O. IZUMI, *Nippon Kinzoku Gakkaishi* **43** (1979) 358.
14. *Idem, ibid.* **43** (1979) 1190.
15. C. T. LIU, C. L. WHITE and J. A. HORTON, *Acta Metall.* **33** (1985) 213.
16. S. KAYA and A. KUSSMANN, *Z. Phys.* **72** (1931) 293.
17. P. LEECH and C. SYKES, *Philos. Mag.* **27** (1939) 742.
18. N. MASAHASHI, T. TAKASUGI, O. IZUMI and H. KAWAZOE, *Z. Metallkde* **77** (1986) 212.
19. B. H. KEAR and H. G. F. WILSDORF, *Trans. Met. Soc. AIME* **224** (1962) 382.
20. R. G. DAVIES and N. S. STOLOFF, *Acta Metall.* **11** (1963) 1347.
21. F. M. C. BESAG and R. E. SMALLMAN, "Ordered Alloys" (Claitor's, Baton Rouge, Los Angeles, 1970).
22. N. S. STOLOFF, *Int. Met. Rev.* **29** (1984) 123.
23. N. MASAHASHI, T. TAKASUGI and O. IZUMI, to be published.
24. H. YOSHINAGA, *Bull. Jpn Inst. Metals* **10** (1971) 519.

Received 2 September
and accepted 12 November 1986